Frontiers in Computing and Intelligent Systems
ISSN: 2832-6024 | Vol. 8, No. 2, 2024

Study on Radiometric Consistency of Landsat Images using Multi-band Joint Regression Model

Yulong Wang, Xiaobang Liu, Li Yu, Chu Wang

The 27th Research Institute of China Electronics Technology Group Corporation, Zhengzhou, Henan 450047, China

Abstract: The long time-series dataset of radiometric consistency is the foundation of image processing, quantitative analysis, image fusion. However, due to the influence of atmospheric conditions, observation angles, geographical environment, reflective-band and other factors, the radiometric inconsistency exist in same-region Landsat images acquired by different satellites or acquired at different times. Therefore, this paper builds the radiation normalization model using Multi-band Joint Regression method, which is used to perform radiometric consistency conversion on Landsat 7/8 images. Meanwhile, the validity of the radiation normalization model is evaluated based on the validation data and vegetation index. Furthermore, the accuracy of the model is verified by comparing with the traditional single-band regression model. Finally, the experiment results show that the proposed model has better accuracy and can enhance the radiometric consistency of multi temporal Landsat images significantly.

Keywords: Radiometric Consistency; Landsat Images; Multi Satellite Sensors; Multi Temporal; Multi Band Joint Regression Model.

1. Introduction

The continuous increase in the number of remote sensing satellites and the open access to remote sensing data with different spatial and temporal resolutions have promoted the comprehensive application of remote sensing data [1]. The time-series observation of multi satellite sensors sensor and multi temporal remote sensing images has become an effective means to quickly and efficiently obtain spatiotemporal distribution and change characteristics such as surface land cover changes, ecological environment monitoring, and quantitative remote sensing inversion [2-5]. However, due to the differences in the observation angle, reflective-band, spectral response ability, atmospheric absorption and scattering, solar illumination geometry and other conditions of different satellite sensors at the observation time, the radiation information of the same ground objects in the same region is inconsistent, resulting in "false changes" on the ground [2, 6-8], which is very unfavorable to the use of time series remote sensing data for change detection. Therefore, it is very important to eliminate the radiometric inconsistency on multi satellite sensors and multi temporal images for forming time-series standard data with continuous time and reliable quality [9].

At present, the radiation normalization methods for multi temporal remote sensing images include absolute radiation normalization and relative radiation normalization [10]. The relative radiation normalization method is the mainstream research, which is proposed based on the linear relationship between the grayscale values of multi temporal image bands [11, 12]. These studies use the same series of satellite images from different research scenes and research areas, and achieve radiation normalization by building radiation conversion models between different sensors. Due to differences in surface and atmospheric conditions, these research results have poor spatial scalability. In addition, the reflectivity differences between sensors may be caused by land cover changes corresponding to inconsistent imaging times, so it is necessary to evaluate these differences using images from the study area [9].

Until now, the Landsat series satellites have been the medium resolution sensors with the longest time span for accumulating satellite data, and these sensors have similar band and spatial resolution parameters. The Landsat series satellite data has been widely used in remote sensing research applications. At present, research on radiation normalization based on Landsat images mainly focuses on areas with high vegetation density and slow surface changes such as tropical rainforests and grasslands, and there is relatively little comparative analysis of medium and high resolution remote sensing images. Therefore, it is urgent and important to evaluate the radiation consistency of Landsat 30 meter resolution images.

This article proposes a radiometric consistency transformation method based on multi band joint regression, and uses multiple sets of Landsat 7-ETM+and Landsat 8-OLI images in the same time period for validation analysis. The purpose of the study is to: (1) analyze the radiation differences between OLI and ETM+ sensors; (2) The impact of the proposed method on the radiometric consistency of OLI and ETM+ images; (3) explore the impact of inconsistent imaging time and vegetation cover changes on the radiometric consistency of Landsat images. This article will provide theoretical support for the radiometric consistency study from remote sensing images in small areas, and also provide data support for the processing and application of long-term remote sensing data.

2. Data and Methods

2.1. Experimental Data

2.1.1. Landsat Remote Sensing Images

This article selects images from the Landsat-7 ETM+ and Landsat-8 OLI sensors. Landsat-7 ETM+ and Landsat-8 OLI both have the same frequency band, including six optical bands (30-meter resolution), one thermal band, and one panchromatic band (15-meter resolution). OLI has a narrower spectral range than ETM+ In the same wavelength range

(Figure 1). In addition, OLI has added shorter blue and infrared cloud bands [13]. The radiation consistency of Landsat images requires the same sensor band, so this article does not involve the blue band and infrared cloud band of OLI. In addition, due to the highly variable spatiotemporal characteristics of the thermal emission process, the conversion of Thermal InfraRed Sensor (TIRS) data between different images is complex and unreliable [14]. Therefore, this article does not analyze the thermal infrared bands of OLI. Finally, this article selects six bands from ETM+ and OLI sensors, including Blue band, Green band, Red band, NIR band, SWIR1 band, and SWIR2 band.

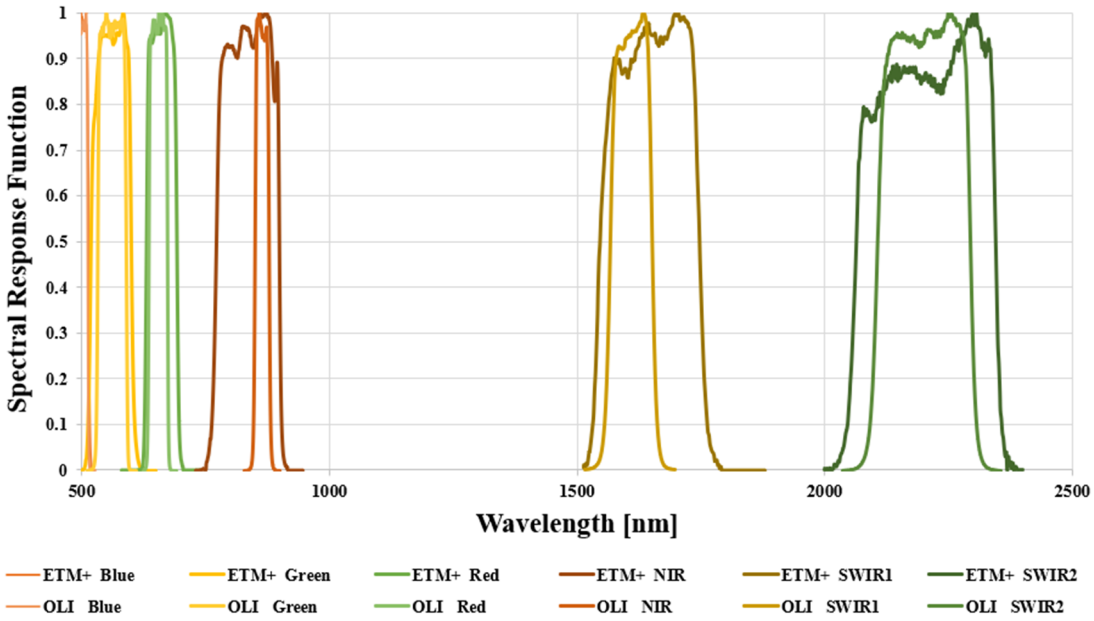

Figure 1. Landsat-7 ETM+ and Landsat-8 OLI spectral response functions

2.1.2. Experimental Data Selection

The Landsat images used in this article are all surface reflectance products that have undergone geometric correction, atmospheric correction, radiation correction, and other processing. To ensure the quality of the selected data, this study sets the following selection principles:

(1) To reduce the impact caused by changes in surface cover or differences in atmospheric conditions, the imaging time difference of Landsat data should not exceed two days;

(2) To ensure the spatial representativeness of Landsat data, the data range covers different regions and land cover types (Figure 2).;

(3) To ensure the temporal representativeness of Landsat data, the time range includes every month from 2016 to 2020.

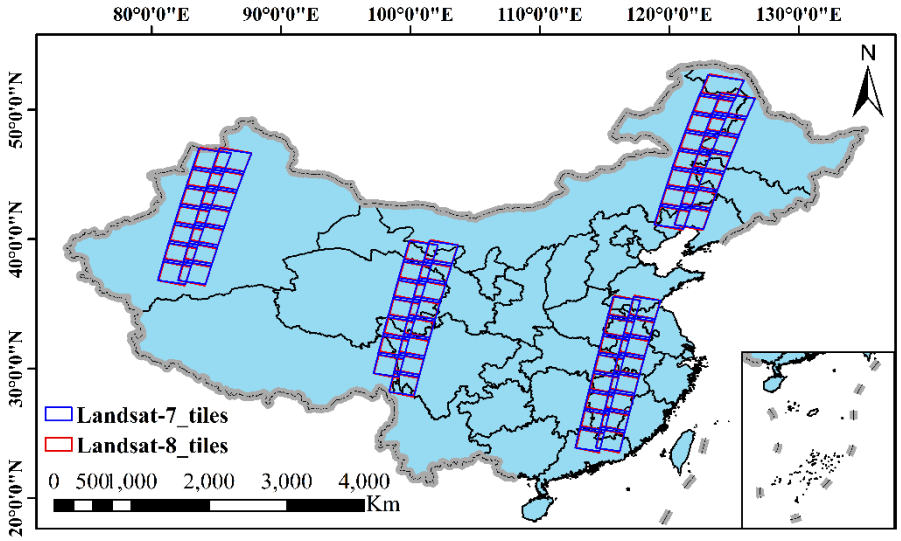

Figure 2. Spatial distribution map of image pairs from Landsat 7/8

2.2. Radiation Normalization Method based on Landsat Data

2.2.1. Rules for Removing Erroneous Pixels

To ensure the quality of Landsat images, it is necessary to remove erroneous pixels, which are caused by factors such as atmospheric pollution, clouds or cloud shadows, sensor limitations, and the presence of SLC off issues with Landsat-7 ETM+. The main methods include: (1) using cloud mask data and the Quality Assessment Band (BQA) to remove cloud shadow or snow pixels; (2) The missing pixels caused by the SLC off of Landsat-7 ETM+ are also removed from the corresponding Landsat-8 OLI pixels. (3) If the pixel of either OLI or ETM+ sensor is saturated, remove the corresponding pixels from both sensors. Based on the above process, this article obtained approximately 2-million-pixel pairs, of which

90% were used for model construction and 10% were used for independent validation.

2.2.2. Multi Band Joint Regression Method

The basic principle of the sensor radiometric consistency conversion model is to assume that there is a linear relationship between the pixel values of multiple temporal images in the same region and the same band. Based on the selected reference image, the reflectance of the image to be converted is normalized to the reference image band by band, thereby reducing the phenomenon of surface "pseudo changes" [2,8]. Roy et al. [12] proposed a consistency transformation to transform between the comparable sensor bands using Ordinary Least Squares (OLS) regression. This article has made improvements in two aspects: (1) This article assumes that all bands of the image to be converted have correlation and complementarity with each band of the reference image. Therefore, this article adopts a multi band joint regression method to predict each band of the reference image using all bands of the image to be converted; (2) When the transformation model is based on least squares fitting, only the error of the image to be transformed is considered, that is, all unmodeled changes are in the dependent variable and not in the reference image. This method is applicable when using the measurement value of one sensor to estimate the measurement value of another sensor [12]. However, in reality, there are also errors in the surface reflectance of the reference image, and noise should exist in any variable rather than only in the independent variable. Therefore, it is more appropriate to use Multiband Orthogonal Distance Regression (M-ODR) for calculating the parameters of the radiometric consistency conversion equation.

The mathematical model for Landsat multi-sensor images radiation regularization based on multi band joint regression method is:

$$Y = AX + B$$

In the formula, matrix Y is the reference image, matrix X is the image to be transformed, matrix A is the parameter of the transformation equation, and matrix B is the constant term of each set of equations, where:

$$Y = \begin{bmatrix} y_1 \\ y_2 \\ y_3 \\ y_4 \\ y_5 \\ y_6 \end{bmatrix}, X = \begin{bmatrix} x_1 \\ x_2 \\ x_3 \\ x_4 \\ x_5 \\ x_6 \end{bmatrix}, A = \begin{bmatrix} a_1 & a_2 & a_3 & a_4 & a_5 & a_6 \\ b_1 & b_2 & b_3 & b_4 & b_5 & b_6 \\ c_1 & c_2 & c_3 & c_4 & c_5 & c_6 \\ d_1 & d_2 & d_3 & d_4 & d_5 & d_6 \\ e_1 & e_2 & e_3 & e_4 & e_5 & e_6 \\ f_1 & f_2 & f_3 & f_4 & f_5 & f_6 \end{bmatrix}, B = \begin{bmatrix} \theta_1 \\ \theta_2 \\ \theta_3 \\ \theta_4 \\ \theta_5 \\ \theta_6 \end{bmatrix}$$

This article uses ODR for multiple linear fitting to obtain matrices A and B, and obtain corrected remote sensing images based on the transformation equation parameters A and B.

3. Experimental Results and Analysis

3.1. Analysis of Multi Band Conversion Model Results

This article uses Landsat 8 OLI as the reference image, substituting the dependent variable Y, Landsat 7 ETM+ as the image to be converted, and inputting the independent variable X. Following the two approaches of single band regression and multi band orthogonal distance regression, the band conversion parameters of the two images are calculated based on single band least squares regression (S-OLS) and multi band joint orthogonal distance regression (M-ODR).

Figure 3 shows the radiation correlation of various bands in the original Landsat-7 ETM+ and Landsat-8 OLI images. The figure shows the consistency and difference between the original bands of two data, with the red line representing the fitted regression line of the two data. Through the regression line and 1:1 line, it can be seen that there are some differences between the original bands of the two data, with the blue band having the worst correlation (R^2= 0.881), the red bands have the best correlation. The RMSE values between the two data are between 0.016 and 0.026, and the slopes of the blue band and SWIR1 have the largest deviation from the 1:1 line, which are both below 0.9.

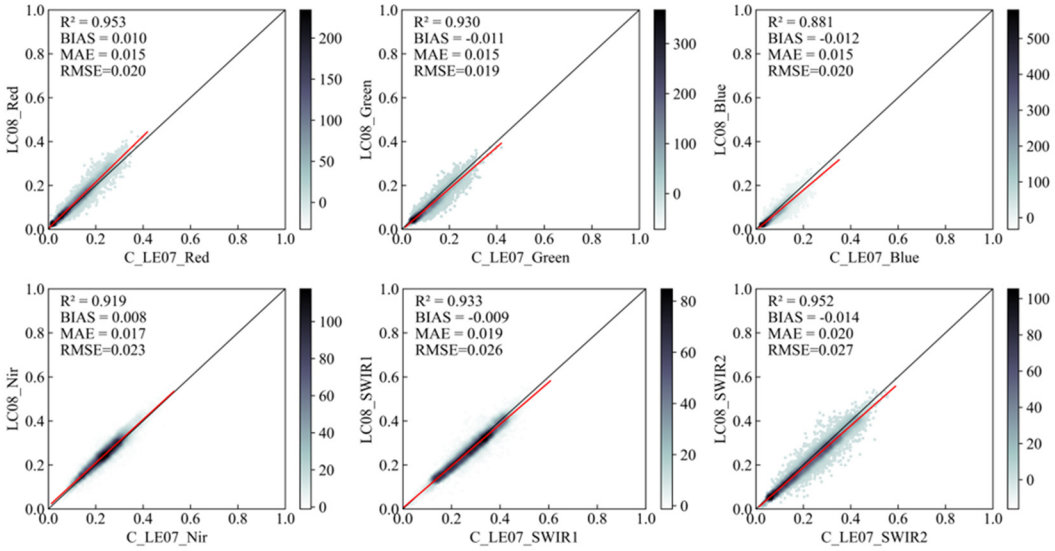

Figure 3. Comparison of raw reflectance between ETM+ and OLI

This article uses the obtained sample pixels as training inputs for model construction, and constructs S-OLS and M-ODR models for ETM+ and OLI band conversion, respectively, to obtain the conversion regression parameters between the two data. Table 1 and Table 2 show the conversion parameters for the S-OLS and M-ODR models, respectively. Use conversion parameters to convert the original ETM+ data to reflectance similar to OLI data, compare the conversion results, and verify the radiation consistency between the original sensor reflectance, S-OLS

model conversion results, M-ODR model conversion results, and baseline data (OLI).

Table 1. S-OLS Regression Conversion Parameters

The Band Name	The S-OLS Conversion Coefficient and Intercept
OLI_Red	0.9656 * ETM_Red - 0.0044
OLI_Green	0.9587 * ETM_Green - 0.0012
OLI_Blue	0.9525 * ETM_Blue - 0.0067
OLI_Nir	1.0030 * ETM_Nir + 0.0045
OLI_SWIR1	0.9535 * ETM_SWIR1 + 0.0049
OLI_SWIR2	0.9555 * ETM_SWIR2 + 0.0030

Figure 4 shows the radiation comparison between ETM+ data and OLI data, where the radiation values of ETM+ data are calculated based on the S-OLS conversion coefficient.

Figure 4 shows the radiation comparison between ETM+ data and OLI data, where the radiation values of ETM+ data are calculated based on the M-ODR conversion coefficient. By comparing the correlation with the original data in Figure 3, both S-OLS and M-ODR models improved the radiation consistency between the two data.

Table 2. M-ODR Regression Conversion Parameter Parameters

The Band Name	The M-ODR Conversion Coefficient and Intercept
OLI_Red	[-0.5780, 0.4115, 0.9665, -0.0388 - 0.0225, 0.0157] / 0.0080
OLI_Green	[-0.5206, 1.1124, 0.1615, 0.0055, -0.0513, 0.0316] / 0.0069
OLI_Blue	[0.1495, 0.4948, 0.0579, -0.0271, -0.0112, 0.0184]/ 0.0001
OLI_Nir	[-0.4978, 0.2105, 0.1033, 0.9571, 0.1265, -0.1269] / 0.0101
OLI_SWIR1	[-0.3482, 0.1683, 0.1363, -0.0382, 0.9591, -0.0606] / 0.0169
OLI_SWIR2	[-0.3342, 0.1959, 0.1087, -0.0450, 0.0127, 0.8860] / 0.0162

In the red, green, and blue bands, the conversion model reduced the deviation between the two data, and the regression line had a higher overlap with the 1:1 line. However, in the S-OLS results, Nir showed a larger deviation than the original data. The results of the M-ODR model show a significant improvement in the overlap between the fitted regression lines and the 1:1 line, indicating that the M-ODR model improves the accuracy of radiative consistency conversion.

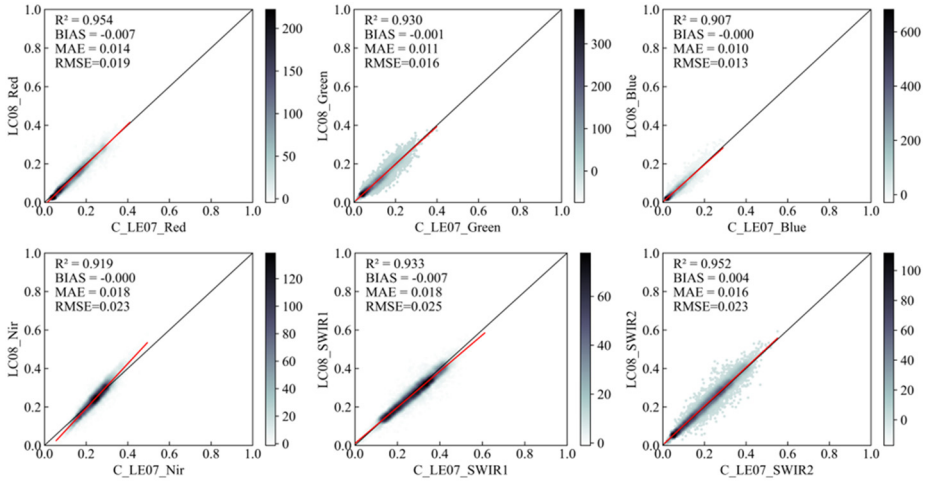

Figure 4. Comparison of surface reflectance in OLI data and ETM+ data after S-OLS model conversion coefficient

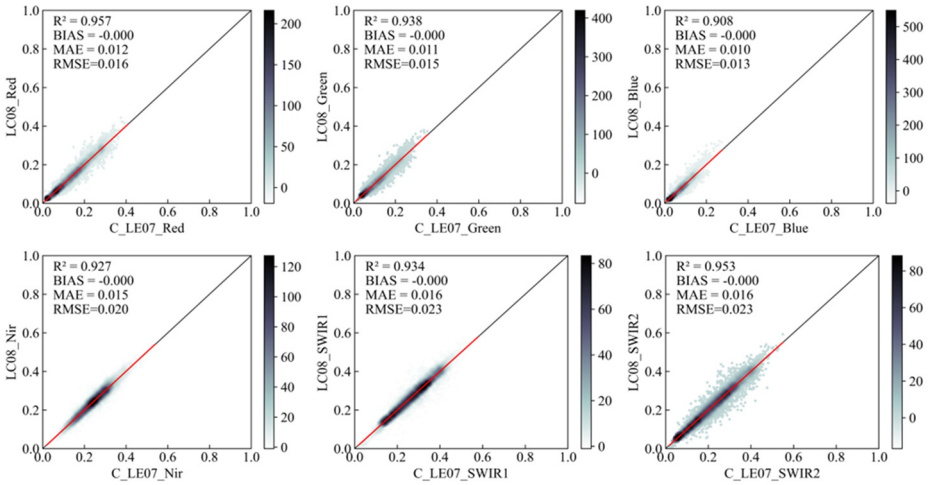

Figure 5. Comparison of surface reflectance in ETM+ data and OLI data after M-ODR model conversion coefficient

Figure 6 quantitatively compares and analyzes the results of the S-OLS and M-ODR models. Compared with the original data, it can be seen that both S-OLS and M-ODR models have achieved improvements in four indicators such

as R^2, Bias, Mae, and EMSE, and the M-ODR model showing the most significant improvement. The above results also prove that in the process of achieving the consistency conversion of different sensors, considering the interaction between bands is conducive to improving band consistency.

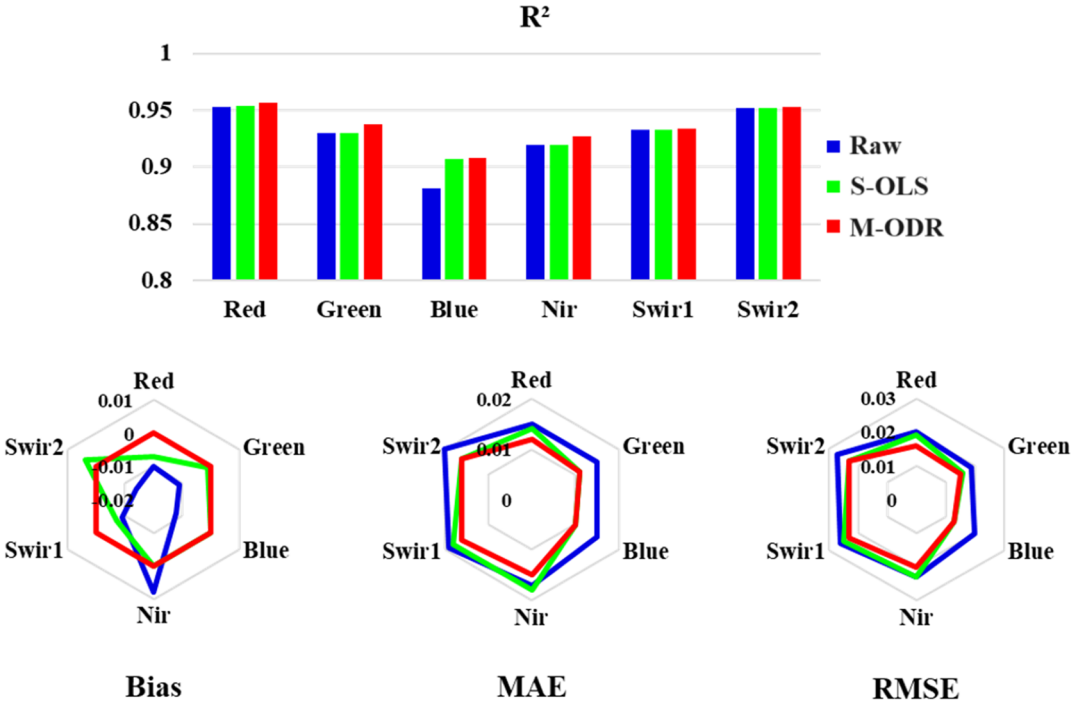

Figure 6. Comparison of data consistency between raw data and S-OLS and M-ODR models after conversion

3.2. The Model Time Sensitivity Assessment of NDVI Index

The spectral bands of sensors have different responses and sensitivities to ground objects. The vegetation index derived from these bands can reduce the uncertainty of atmospheric correction and the sensitivity to satellite angle changes, and at the same time, it is often used as an evaluation variable for conversion and calibration between different sensors [15]. Therefore, by comparing and analyzing the consistency of NDVI values before and after band conversion in different seasons, this article aims to verify the performance and effectiveness of the band conversion model in improving the consistency between bands.

Figure 8 shows the evaluation results of NDVI calculated using the transformation model. The M-ODR model has a significant advantage in improving the consistency between data, reducing the deviation value of the original data from 0.04 to 0.00, indicating that the reflectance obtained by the transformation model improves the consistency of estimating NDVI and significantly reduces the deviation between data.

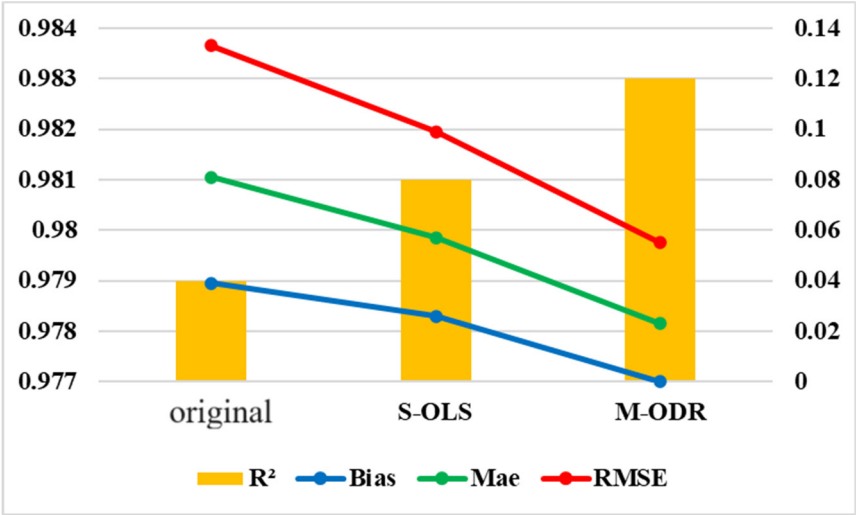

Figure 7. Correlation statistics between NDVI of ETM+ and OLI after raw and band conversion

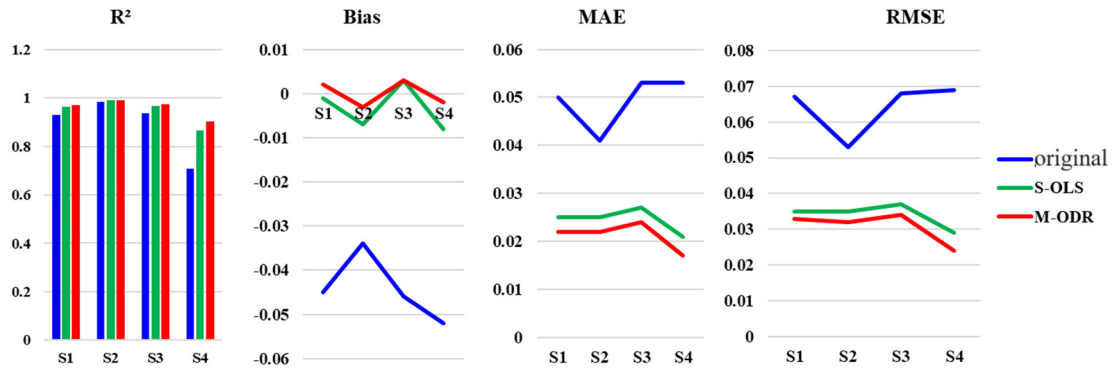

Figure 8. Comparison of NDVI correlation between original and band converted ETM+ and OLI under different seasonal conditions

In addition, this study found a temporal correlation between the radiation consistency of Landsat-7 ETM+ and Landsat-8 OLI data. In summer, the radiation consistency of data is highest, followed by spring and autumn, while in winter, the radiation consistency of data is lowest. The reason for this phenomenon is that summer is the peak period of vegetation growth, with the largest vegetation coverage area. At this time, the reflectivity is less affected by the vegetation background, so the correlation of sensitive bands to vegetation increases. However, in the non vegetation growth period, the surface background is complex, and the reflectivity is affected by the complex surface, resulting in a decrease in correlation.

In this study, both single band conversion models and multi band conversion models were able to achieve radiation consistency conversion between Landsat-7 ETM+ and Landsat-8 OLI, and improved the radiation consistency between raw data. The results of independent validation data indicate that the reflectance obtained by the multi band conversion model considering the correlation between data has higher consistency.

4. Conclusion

In this paper, a conversion model based on multi band joint regression is proposed to achieve the conversion of radiation consistency between different data. The results show that the method can improve the accuracy of model conversion by considering the correlation between bands, and the multi band conversion model based on orthogonal distance regression has better robustness. Compared with the single band conversion model, the converted results show better consistency. The validation results of the conversion model using vegetation indices also demonstrate that the M-ODR model proposed in this paper has good conversion accuracy.

The multi band conversion model of orthogonal distance regression can realize the consistent conversion of multi-sensor radiation, and realize the fast conversion of different sensor data. By constructing the radiation consistency conversion model of different sensors, it is beneficial to reduce the radiation difference between sensors, facilitate the construction of time continuous and radiation consistent remote sensing reflectance data, and provide long-term radiation consistent data for remote sensing data time series research and application.

References

[1] Huang Liting, Jiao Weili, et al. Radiometric Normalization of GF-1 Imagery Based on Regularized IR-MAD [J]. Remote Sensing Information. 2020, 35(3):11.

[2] Jiang Sili, Huang W, et al. Thick cloud removal of remote sensing images based on multi-reference image information fusion [J]. Remote Sensing for Natural Resources, 2022, 34(2):121-127.

[3] Cao Wenting. Long-term Continuous Monitoring of Island Urbanization and Its Ecological Consequences [D]. Zhejiang university, 2020.

[4] CAO H, HAN L, LI L. Harmonizing surface reflectance between Landsat-7 ETM +, Landsat-8 OLI, and Sentinel-2 MSI over China [J]. Environ Sci Pollut Res Int, 2022.

[5] LI P, JIANG L, FENG Z. Cross-Comparison of Vegetation Indices Derived from Landsat-7 Enhanced Thematic Mapper Plus (ETM+) and Landsat-8 Operational Land Imager (OLI) Sensors [J]. Remote Sensing, 2014, 6(1): 310-29.

[6] Zhan Jun, Li Dan. Application of the Pseudo-invariant Feature Method for Image Relative Radiometric Normalization Process [J]. Geomatics & Spatial Information Technology, 2023(7):3.

[7] Huang Qiting, Tan Zelin, et al. A Study on the Relative Radiometric Normalization of Multi-sources and Multi-temporal Remote Sensing Data [J]. Journal of Geo-information Science, 2016, 18(5): 606-614.

[8] Bai Yang. Radiometric Normalization of Remote Sensing Image Based on Kernel Canonical Correlation Analysis [D]. The University of Chinese Academy of Sciences, 2018.

[9] MANIVASAGAM V S, KAPLAN G, ROZENSTEIN O. Developing Transformation Functions for VENμS and Sentinel-2 Surface Reflectance over Israel [J]. Remote Sensing, 2019, 11(14).

[10] Yu Xiaomin, Zhou Qin. Methods of Radiometric Normalization for Multi-Temporal Remote Sensing Images: A Review [J]. Geomatics & Spatial Information Technology, 2012 (6):5.

[11] CHASTAIN R, HOUSMAN I, GOLDSTEIN J, et al. Empirical cross sensor comparison of Sentinel-2A and 2B MSI, Landsat-8 OLI, and Landsat-7 ETM+ top of atmosphere spectral characteristics over the conterminous United States [J]. Remote Sensing of Environment, 2019, 221: 274-85.

[12] ROY D P, KOVALSKYY V, ZHANG H K, et al. Characterization of Landsat-7 to Landsat-8 reflective wavelength and normalized difference vegetation index continuity [J]. Remote Sensing of Environment, 2016, 185: 57-70.

[13] Xu Guangzhi, Xu Hanqiu. Cross-comparison of Sentinel-2A MSI and Landsat 8 OLI Multispectral Information [J]. Remote Sensing Technology and Application, 2021(1):11.

[14] Wang Jingrui, Wei Xinyuan, et al. Assessing Relative Radiometric Normalization Performances of Surface Brightness Temperature from Multi-temporal Landsat Images [J]. Remote Sensing Information, 2016(2):7.

[15] Xu feng, Li Hengkai. Cross-comparison of Landsat TM/OLI and HJ-1B CCD Sensor Data [J]. Remote Sensing Information, 2021(4):9.